RSC Advances

RSC Publishing

PAPER

View Article Online
View Journal | View Issue

Fluid propulsion using magnetically-actuated artificial cilia – experiments and simulations

Cite this: *RSC Advances*, 2013, **3**, 12735

Syed Khaderi,[a] Jeanette Hussong,[b] Jerry Westerweel,[b] Jaap den Toonder[c] and Patrick Onck*[d]

Received 3rd March 2013,
Accepted 13th May 2013

DOI: 10.1039/c3ra42068j

www.rsc.org/advances

We conducted a combined modelling and experimental approach to explore the underlying physical mechanisms responsible for fluid flow caused by magnetically-actuated plate-like artificial cilia. After independently calibrating the elastic and magnetic properties of the cilia, the model predictions are observed to be in excellent agreement with the experimental results. We show that the fluid propelled is due to a combination of asymmetric motion and fluid inertia forces. The asymmetric motion of the cilia and inertial forces contribute equally to the total fluid flow. We have performed a parametric study and found the cilia thickness and magnetic field that should be applied in order to maximise the fluid transport.

1 Introduction

One of the important components of a lab-on-a-chip (LOC) is the fluid propulsion system that transports the fluid to be analysed through the microchannels. Due to the large surface to volume ratios that occur at the small length scales of typical LOCs conventional methods no longer suffice, which has led to a search for new methods to propel fluids. This has resulted in magneto-hydrodynamic and electro-osmotic pumps and bio-inspired pumping mechanisms that mimic natural fluid propulsion systems at the micrometer length scale. The flows created by magneto-hydrodynamic pumps and electro-osmotic pumps depend strongly on the electro-kinetic properties of the fluid to be propelled. Moreover, the electric fields used in these devices can cause heating, bubble formation and interact with the biofluid to be analysed, thereby polluting the analyte. Recently, researchers have used the principles used by natural ciliates to design mechanical actuators (*i.e.* artificial cilia) that can create fluid transport in microchannels. The artificial cilia are actuated by various external triggers, including piezo actuation,[16] light[20] electric[3] and magnetic[2,5,6,8–12,17,18] fields. A review of various approaches to propel fluids using artificial cilia can be found elsewhere.[4] Some of the aforementioned actuation techniques have certain disadvantages. For instance, electric fields can interact with the biofluid to be analysed, the response time for light actuation can be very large and achieving asymmetric motion is difficult in the case of piezo actuation. The magnetically driven cilia systems do not suffer from these drawbacks, and hence, have potential for microfluidic fluid propulsion.

In general, the fluid transport by artificial cilia can be due to (1) spatial asymmetry, and in the presence of fluid inertia, due to (2) temporal or (3) orientational asymmetry.[9] The spatial asymmetry is due to the non-reciprocal motion of the cilia during the effective and recovery strokes. The temporal asymmetry can be achieved when the velocities of the effective and recovery strokes are different. Orientational asymmetry will be present when the mean position of the cilia is inclined at an angle to the axis of the microchannel.

In the Stokes regime, the fluid transport by magnetic artificial cilia is governed by the competition between the elastic forces of the cilia and the viscous and magnetic forces acting on it. Using numerical simulations,[10] it has been shown that the amount of spatial asymmetry exhibited by super-paramagnetic cilia, and hence the fluid transport, is increased when the magnetic forces are high and when the viscous forces are low. The spatial asymmetry was achieved due to the interaction of a rotating magnetic field with the super-paramagnetic cilia. In contrast to natural cilia, the recovery stroke was observed to be faster compared to the effective stroke (temporal asymmetry). The flow transported by the cilia also depends on geometric parameters such as the cilia spacing and the channel height.[11] When the width of the channel is large in comparison to the height, the fluid propelled increases when the height of the channel is increased, and also when the cilia spacing is decreased.

Natural cilia also beat in a coordinated manner so that neighbouring cilia beat out-of-phase, thereby generating metachronal waves. The effect of such an out-of-phase motion of magnetically actuated cilia has also been investigated.[7,12,13]

[a]*Department of Engineering, Cambridge University, Cambridge, UK*
[b]*Laboratory for Aero and Hydrodynamics, Delft University of Technology, Delft, The Netherlands*
[c]*Eindhoven University of Technology, Eindhoven, The Netherlands*
[d]*Zernike Institute for Advanced Materials, University of Groningen, Groningen, The Netherlands. E-mail: p.r.onck@rug.nl*

In the presence of spatial asymmetry,[7,12] the out-of phase motion leads to a significant increase in the net fluid transported compared to uniformly beating cilia. Studies on the flow created by cilia that beat with metachrony but without spatial asymmetry[13] show that metachronal motion alone can also create fluid flow. However, realising a magnetic actuation system that can create an out-of-phase motion of cilia is rather challenging from a technical point of view.

In nature, the length of cilia is on the order of 10 μm, and they beat with a frequency of 10 Hz. As a result, the Reynold's number is $\approx 1 \times 10^{-3}$, and the effect of fluid inertia is negligible in comparison to the effect of viscous forces in the fluid. The fabricated artificial cilia are typically 100 μm long; in addition the beat frequency can also be externally tuned (10 Hz–100 Hz). Hence, for artificial cilia, the influence of fluid inertia cannot be neglected. This effect was first investigated for electrically actuated artificial cilia,[1,3] in the context of microfluidic mixing. It was shown that mixing of fluids can be enhanced in the presence of fluid inertial forces. Motivated by these studies, the effect of fluid inertia on the fluid transport was studied,[14] showing that larger Reynold's numbers lead to larger flows.

Based on these studies, plate-like artificial cilia have been fabricated and integrated into a microfluidic channel.[2] The aforementioned theoretical studies on the magnetically driven artificial cilia are based on a uniform distribution of the magnetic field. Realising such uniform magnetic fields experimentally involves an elaborate design of the actuation system.[6,17,21] Alternatively, a simple actuation system was proposed using a non-uniform magnetic field, created by a rotating permanent magnet.[2,8] Fluid flow measurements performed show that the velocities generated by the cilia subject to such non-uniform magnetic field can reach values around ≈ 130 μm s^{-1}.[8] However, the underlying physical mechanisms that are responsible for these fluid velocities remain unclear. The main objective of the current article is therefore to identify the dominant cause for the breaking of asymmetry leading to flow and to relate this to the non-uniform magnetic field generated by the rotating permanent magnet. Moreover, we will identify the combination of system parameters that will lead to maximum fluid transport.

The article is organised as follows. The set of experiments used to characterise the elastic and magnetic properties of the cilia are explained in section 2. The numerical method and geometry used for the analysis is described in section 3. In section 4, various factors that influence the fluid transport are explored. Finally, the conclusions are summarised in section 5.

2 Experimental setup

An array of artificial cilia was fabricated using a composite of poly(*n*-butylacrylate) (P*n*BA) containing photoreactive side groups and super-paramagnetic magnetite nano-particles (with particle diameter 10–20 nm and volume fraction

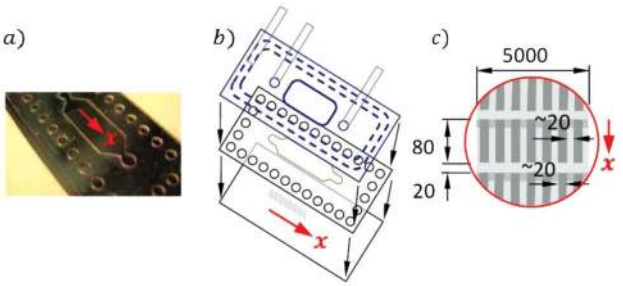

Fig. 1 (a) Picture of the substrate and placed cartridge. The cilia area covers the whole channel section of 5 × 10 mm^2. The transport direction of the cilia is indicated with a red arrow. (b) Schematic of the channel with three components: the ciliated substrate in the bottom, the middle cartridge and the channel cover with integrated fluid connections and the vacuum channel. (c) Schematic of the cilia array. All dimensions are in μm. The dimension of 80 μm refers to the length of cilia (70 μm) and the region fixed to the substrate (10 μm). Approximately 10000 individual rectangular-shaped structures are distributed over the channel bottom.

$\approx 9\%$).[2] These artificial cilia are flap-shaped with length L = 70 μm, width b = 20 μm and thickness h = 0.9μm, elastic polymer structures that are attached at one end to the substrate surface of a silicone wafer. The cilia are located 20 μm apart (along the width direction) while the streamwise distance (along the length direction) from cilia tip to cilia tip equals 100 μm. To create a microfluidic chamber around the cilia, a channel is assembled on top of the cilia-covering substrate in a sandwich-like system (see Fig. 1). A cartridge made of poly(*N*,*N*-dimethylacrylamide) of 500 μm thickness is placed on the substrate surface. The cartridge has a rectangular void of 10 mm length and 5 mm width in its middle which defines the side walls of the fluid channel. The channel is closed by placing a glass cover on top of the cartridge. The glass cover has integrated inlet and outlet channel connections, therefore allowing to fill the channel after assembly with fluid. All three components are hold together by clamping. Additionally, a connection to a vacuum channel allows sealing the microfluidic channel by under pressure during usage. A rotating permanent magnet of dimensions 10 mm × 25 mm × 50 mm that is placed below the channel is used to actuate the cilia, see Fig. 2. The magnetization of the magnet is determined by comparing the field caused by the magnet with the field created by a rectangular permanent magnet.[14]

The following set of experiments are performed under quasistatic conditions using the same batch of cilia as reported in[8] to provide input to the numerical model to estimate the elastic and magnetic properties of the cilia. (1) The array of cilia is subjected to an external flow in the absence of the permanent magnet and the projected length of the cilia observed from the top view of the channel is measured (the 'applied flow' case). (2) The projected length of the cilia is measured for various orientations of the permanent magnet (quasistatic loading) with no external flow imposed (the 'applied field' case). The deflection of the cilia in

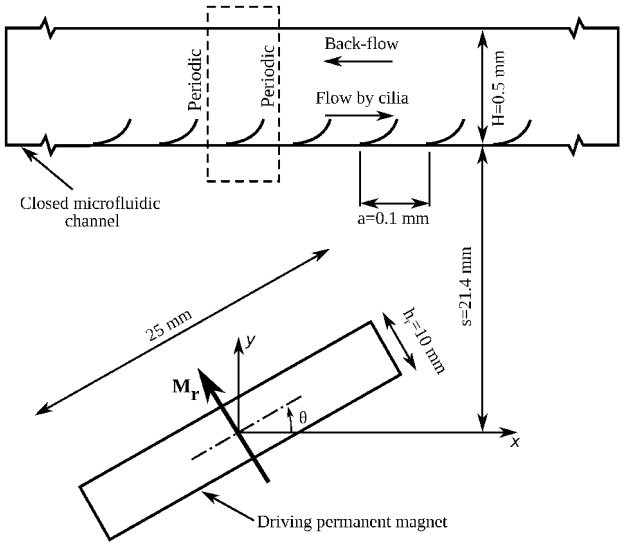

Fig. 2 Experimental set-up used to study the fluid transport due to artificial cilia (not to scale). Magnetic cilia of length 70 μm, spaced 100 μm apart are used to create a flow in a closed channel of height 0.5 mm, width 5 mm and length 20 mm. The artificial cilia are driven using a permanent magnet having a remnant magnetization $\mathbf{M_r}$ that rotates about the *z* axis.

the applied flow experiments is a direct measure of the elastic properties, while the results from the applied field experiments are used to characterise the magnetic properties of the cilia.

Phase-locked micro-particle image velocimetry measurements were performed at 20 different phases throughout an actuation cycle to quantify the instantaneous velocity distributions of the flow in bottom parallel measurement planes. Measurements were performed in a stack of 20 planes with a spacing of 20 μm between each plane. To increase the reliability of the measurement results compared to instantaneous vector results, ensemble averages were computed for each vector field from a set of 100 image pairs. The measurement region spans an area of 400 × 300 μm, therefore covering a field of approximately 30 individual cilia. Measurements are performed at the channel symmetry plane such that sidewall effects in the measurement result can be neglected.

3 Computational model

We model the cilia as elastic Euler–Bernoulli beams, taking into consideration geometric non-linearity and inertia of the cilia in a two-dimensional Lagrangian framework. By using a two-dimensional model, we neglect the spacing between the cilia in the out-of-plane direction (Fig. 2) and assume that the cilia span the entire width of the channel. Experiments[8] indicate that this is permissible since the cilia are close enough to ensure that the velocity field is uniform along the channel width. This is also supported by the three-dimensional simulations of cilia,[15] where it is shown that the velocity field across the width is uniform even when the spacing (along the channel width) between the cilia is more than 4*b*. The magnetic field is calculated by solving the Maxwell's equations using a boundary element approach for each ciliary configuration. The Navier–Stokes equations are solved within an Eulerian setting for the velocity and pressure using finite elements. The velocity is interpolated quadratically, while the pressure is interpolated linearly within each element. The solid-fluid coupling is performed by imposing the velocity of the cilia to be equal to the velocity of the fluid. This condition is enforced at the nodal points of the Euler–Bernoulli beam elements using Lagrange multipliers (point collocation method) within a fictitious domain framework.[19] Details concerning the governing equations and numerical implementation can be found in Khaderi *et al.*[14] The solution procedure can be summarised as follows. The Maxwell's equations are solved at every time instant to solve for the magnetic field, from which the magnetic body couple acting on the cilia is calculated. This body couple is provided as an external load to the implicitly-coupled solid-fluid model, which simultaneously solves for the cilia velocity, and the velocity and pressure of the fluid. The velocity of the cilia is integrated using Newmark's algorithm to calculate its new position, and this procedure is repeated.[14]

Motivated by the experimental parameters, a periodic unit-cell of width 0.1 mm and height 0.5 mm containing one cilium is used for the simulations (see Fig. 2). The cilia have a length $L = 70$ μm, thickness $h = 2$ μm and a width $b = 20$ μm. The fluid has a viscosity of $\mu = 1$ mPa and a density of $\rho_f = 1000$ kg m^{-3}. No-slip boundary conditions are applied to the top and bottom of the channel. The initial configuration of the cilia is not exactly known from the experiments. Hence, the initial configuration is chosen to be an arc of a circle of length L with the height of the segment equal to aR, where R is the radius of the circle (see Fig. 3(a)). In the simulations, the fixed edges of the cilia are placed $h/2$ above the no-slip boundary, to mimic the presence of the sacrificial layer used during the manufacturing process.[3] The other input quantities of the numerical model are the elastic and magnetic properties. To obtain the elastic and magnetic properties of the cilia, we use the numerical model to match the experiments as discussed in section 2.

The elastic modulus depends on the amount of cross linker used in the polymer films, and on the duration of exposure to ultra-violet radiation during cilia processing. The elastic modulus of the cilia is estimated by comparing the simulated projected length of the cilia with the results of the applied flow measurements. The flow is imposed by specifying a flux on the left boundary of the periodic cell. The simulation results match with the experimental data for an elastic modulus of 0.65 MPa, see Fig. 3(b). The initial configuration used is a circular arc segment with $a = 0.7$ rotated by $\phi = -10^\circ$, see Fig. 3(a).

To determine the magnetic field caused by the permanent magnet we have to know its magnetization $|\mathbf{M_r}|$. The following procedure is adopted to estimate the magnetization of the

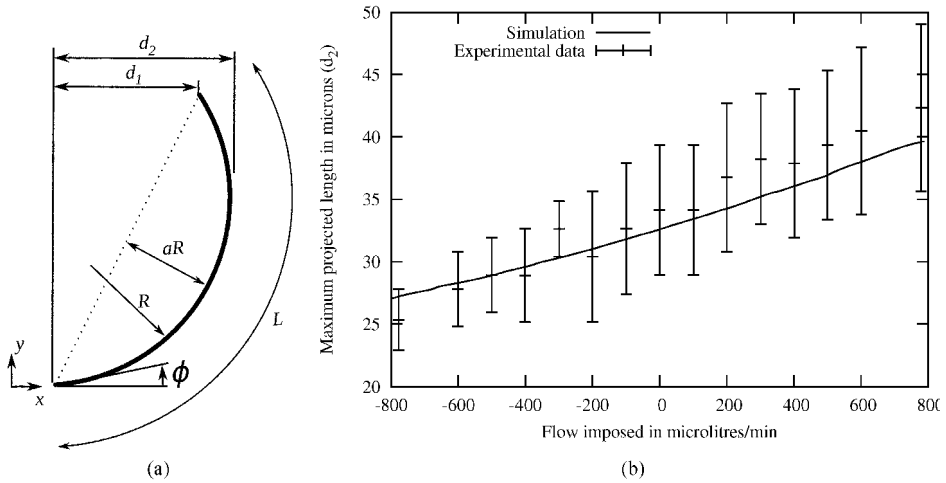

Fig. 3 (a) The initial configuration chosen is an arc of a circle with a length L. Here, d_1 is the projected distance between the two ends of the cilia and d_2 is the maximum projected length of the cilia (as seen from the top of the channel). (b) Comparison between the experimental and simulated maximum projected lengths (d_2) when the elastic modulus is 0.65 MPa and a = 0.7 rotated by $\phi = -10^\circ$.

rotating permanent magnet. The y-component of the magnetic field created by the permanent magnet was measured just above the magnet at y = 21.4 mm (Fig. 2) using a Gauss meter and its variation with θ is shown in Fig. 4. The analytical solution for the magnetic field created by a rectangular permanent magnet[14] was compared to the experimentally measured field, and a good match was obtained for a magnetization of 1.27 MA m^{-1} (Fig. 4).

For the simulations of the applied field case, no flux is specified on the left boundary. The projected length data from the applied field measurements were used (Fig. 5) to estimate the magnetic susceptibility by matching the projected length of the cilia for different orientations of the magnet under quasistatic conditions. The measurements were performed halfway between the channel inlet and outlet. The simulated projected length for an isotropic magnetic susceptibility of 0.08 is shown in Fig. 5. The initial configuration used is a circular segment with a = 0.7 and $\phi = 10^\circ$. We conjecture that the main source of the differences comes from the uncertainty in the initial configuration.

The flow caused by the cilia is due to the competition between magnetic forces, elastic forces of the cilia, fluid viscous and inertia forces. Consequently, three physical dimensionless parameters can be identified:[14] (i) the fluid number $F_n = (\mu/12Et_{\text{beat}})(L/h)^3$-the ratio of viscous to elastic forces, (ii) the Reynold's number $Re = \rho_f L^2/t_{\text{beat}}$-the ratio of fluid inertial to viscous forces and (iii) the magnetic number $M_n = (\mu_0 H_0^2/12E)(L/h)^2$-the ratio of magnetic to elastic forces. Here, t_{beat} is the time taken by the cilia to complete one beat cycle and is equal to half the time period of the rotating magnet, μ_0 is the magnetic permeability in vacuum and H_0 is the magnetic field caused by the permanent magnet. By assuming that the magnet can be approximated as a dipole,

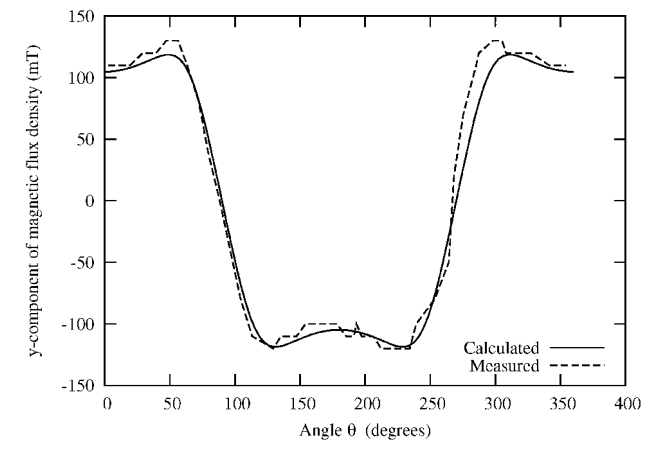

Fig. 4 Comparison of the measured and calculated magnetic field for a magnetization of 1.27 MA m^{-1}.

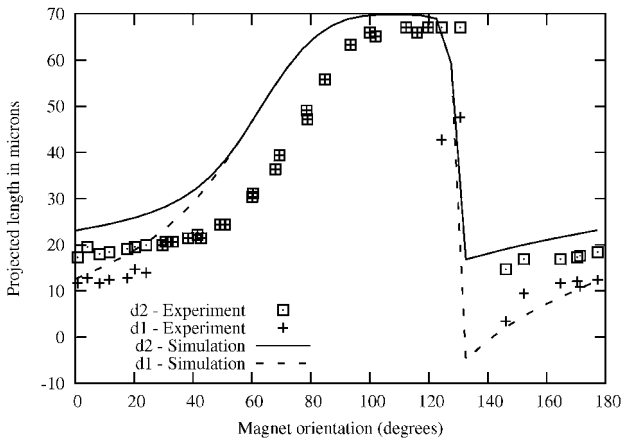

Fig. 5 Comparison between the experimental and simulated projected lengths for an isotropic magnetic susceptibility of 0.08. The dimensions d_1 and d_2 are illustrated in Fig. 3(a).

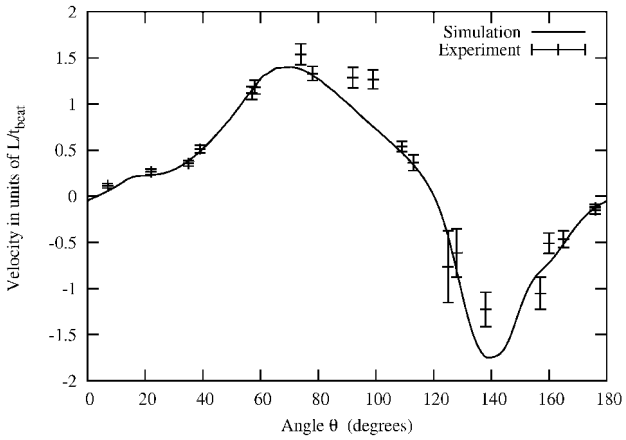

Fig. 6 Velocity at a plane 60 microns from the base during a half magnet rotation at 10 Hz.

whose magnetic field decreases as $1/r^3$ with distance r, H_0 is taken to be of the form $|M_r|(h_r/2s)^3$, where h_r is the thickness of the rotating magnet and s is the distance between the magnet and the microfluidic channel (see Fig. 2). The relevant geometrical dimensionless parameters are H/L and a/L, where H is the height of the microfluidic channel and a is the cilia spacing along length. The dimensionless parameters, when the frequency of the rotating magnet is 10 Hz, are $F_n = 1.21 \times 10^{-3}$, $M_n = 0.281$, $Re = 0.098$, $H/L = 7.14$ and $a/L = 1.42$.

4 Results

As we have now calibrated the elastic and magnetic properties of the cilia and found the magnetization of the actuating permanent magnet, we are in a position to perform simulations to capture the flow generated by the cilia. To simulate the closed channel, a zero-flux condition is imposed on the periodic edges of the unit-cell (see Fig. 2). Since we simulate a single cilium in a periodic domain, this model implicitly neglects the phase lag between the cilia due to a possible non-uniform magnetic field as observed by Belardi *et al.*[2] The data points in Fig. 6 show the time evolution of the instantaneous horizontal velocity† at a plane 60 microns (=0.85 L) from the substrate for a frequency of 10 Hz. The initial configuration used is an arc of a circle with $a = 0.7$ and $\phi = -10^\circ$. As shown in Fig. 6, there is a good agreement between the numerical and experimental data.

Fluid transport by artificial cilia can be due to (1) spatial asymmetry, (2) temporal asymmetry and (3) orientational asymmetry. The relative contribution of temporal and orientational asymmetry is difficult to identify in the presence of inertia, and we therefore combine these two effects into an 'inertia-induced' contribution, in addition to the 'spatially-induced' contribution. In the following we analyse which of these contributions is dominant in causing the net fluid transport. To ascertain if there is a spatial asymmetry, we have to observe the cilia motion from the side of the channel. As this is a difficult task experimentally due to restricted optical access, we resort to the simulations to analyse this. Fig. 7 shows the deformed shape of the cilia for various time instances. The circular arrows at the two ends of the cilia represent the direction of the magnetic body couple acting on the respective ends. It can be seen that when the magnet turns by 180°, the cilia complete one beat cycle (t_{beat} is half the time period of the rotating magnet). To analyse the area swept by the cilia, we plot the trajectory of the tip of the cilia in Fig. 7, with the straight arrows showing the direction of motion. It can be clearly seen that the cilia exhibit a spatially asymmetric motion during a beat cycle with the rotation of cilia tip in a

† The instantaneous velocity in the simulations was calculated as, $\int u_x(y = 60\ \mu\text{m}, t)dx/a$ where a is the spacing between the cilia and μ_x is the velocity in the x direction.

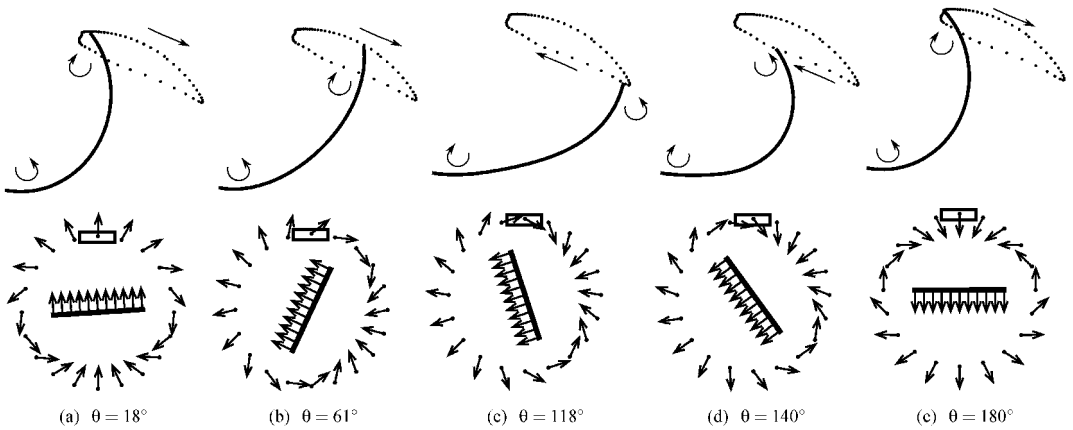

Fig. 7 Configuration of cilia at various time instances. The top figure shows the deformed geometry of the cilia and the dots show the trajectory of the tip of the cilia. The straight arrows, curved arrows and dots represent the direction of the cilia motion, the magnetic body couple and the trajectory of the tip, respectively. The bottom figure shows the orientation of the magnet and the distribution of magnetic field in a circle around the magnet. The box represents the microchannel that contains the cilia.

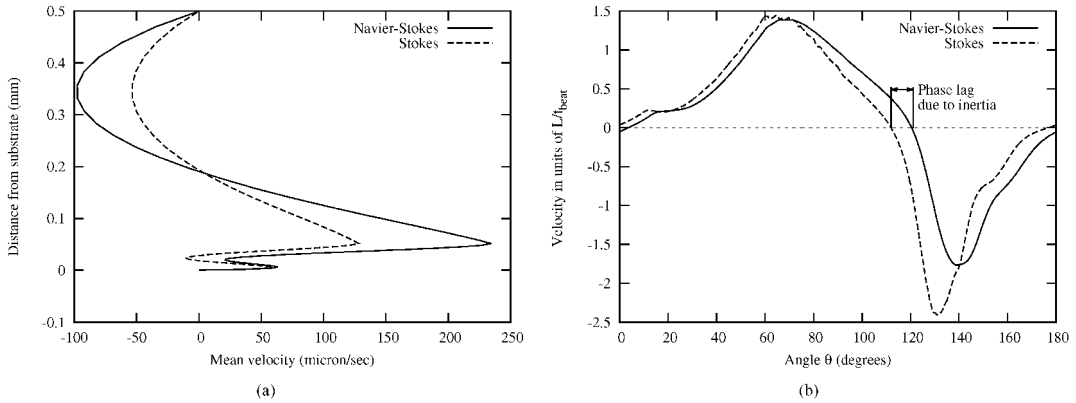

Fig. 8 Effect of fluid inertia: (a) Mean velocity profile at 10 Hz. (b) Velocity at a plane 60 microns from the base during half a magnet rotation at 10 Hz.

direction opposite to that of the magnet during the effective stroke. During the effective stroke, a counter-clockwise/clockwise torque acts on the cilia near the fixed/free end. This straightens-up the cilia and enables the cilia to follow the magnetic field during the effective stroke to the right, see Fig. 7(a) and (b). As the cilia cannot continue to follow the magnetic field forever, due to the elastic forces and due to the presence of the channel walls, they become locked momentarily while the magnetic field keeps on rotating, see Fig. 7(c). As the magnetic field continues to rotate, the magnetic torque is reversed such that a counter-clockwise/clockwise torque act on the cilia near the free/fixed end, see Fig. 7(d) and (e). This makes the cilia more curved as they return to the initial position. We note that the effective stroke takes place during the first $\approx 111^\circ$ rotation of the magnet, leading to a positive velocity. As the magnet continues to rotate further, the recovery stroke takes place, which leads to a negative velocity. The mean velocity of the recovery stroke is about 1.5 times larger than that of effective stroke.

Fig. 7 clearly shows that the cilia exhibit a spatially asymmetric beat cycle, which contributes towards a net fluid flow even in the absence of fluid inertia. To explore whether temporal or orientational asymmetry also contribute to the net flow, we now investigate the effect of inertial forces.

4.1 Effect of fluid inertia

To see if there is any effect of fluid inertia on the fluid transported we performed simulations in which the inertia terms in the Navier–Stokes equations were neglected. The results are plotted in Fig. 8. The spatial asymmetry, *i.e.* the area swept by the cilia was found to be identical in the presence and absence of fluid inertia. The results show that the fluid inertia plays an important role even at low frequencies of 10 Hz and a cilia length of 70 micron (corresponding to a Reynold's number $\rho L^2/\mu t_{\text{beat}} = 0.098$). The mean velocity profile shows that the maximum fluid velocity in the absence of inertia (due to the spatial asymmetry) is nearly half that of the flow in the presence of inertia at some elevations (see Fig. 8(a)). The instantaneous velocity at an elevation of 60 micron is compared for Stokes and inertial flow in Fig. 8(b). The effect of fluid inertia is to increase the positive velocity and decrease the negative velocity‡. The cause of this increased positive flow can be understood by comparing the velocity contours of the Stokes and inertial flows, at the instant when the cilia reverse their motion, from the effective stroke to the recovery stroke. This happens at $\theta \approx 111^\circ$. The velocity contours are shown in Fig. 9 for Stokes and inertial regimes. In the absence of the inertia forces (Fig. 9(a)), the fluid instantaneously follows the cilia motion, and this results in a negligible fluid velocity when the cilia reverse their motion (see also Fig. 8(b) at $\theta = 111^\circ$). In the presence of the inertia forces, the fluid continues to flow to the right (positive velocity) even when the cilia have reversed the direction (moving to the left) (Fig. 9(b)), thereby resulting in an inertia-induced phase lag as marked in Fig. 8(b). This

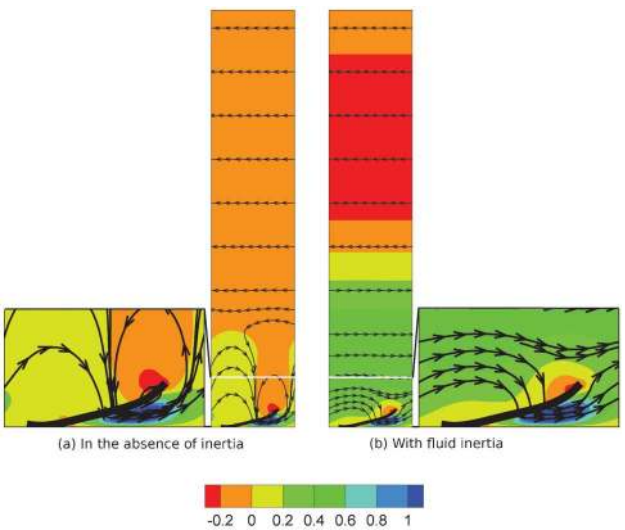

Fig. 9 Comparison of velocity field at the beginning of the recovery stroke ($\theta = 111^\circ$) in the (a) absence and (b) presence of fluid inertia. The contours represent the velocity in the channel direction in mm s^{-1}. The white line represents the elevation of 60 microns.

‡ No significant differences were observed in the area swept and the cilia velocity between the results presented in Fig. 8.

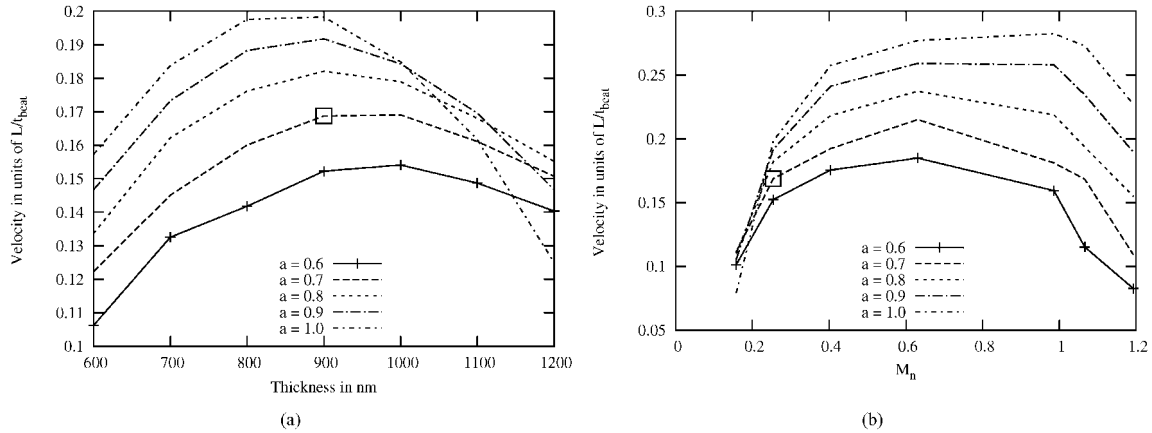

Fig. 10 Mean velocity at an elevation of 60 microns from the substrate as a function of the (a) cilia thickness and (b) magnetization of the permanent magnet for different choices of initial configurations. The flow created by the present experimental system is shown using the square symbols.

increases the magnitude of fluid propelled to the right during the effective stroke. In the presence of fluid inertia, localisation of velocity occurs near the cilia during the fast recovery stroke (as also seen elsewhere[14]). This results in a reduction in the magnitude of maximum negative velocity for the inertial flow compared to the Stokes flow (Fig. 9(b)).

4.2 Parameters for optimal flow

In this section we explore the effect of the system parameters in order to create a maximum net fluid velocity. To this end, we study the mean fluid velocity in a cycle at an elevation of 0.85 L from the substrate as a function of magnetization ($M_r = |\mathbf{M_r}|$) and cilia thickness for different initial configurations (by changing the values of a in Fig. 3(a) with the cilia rotated by $\phi = -10^{\circ}$). The results are presented in Fig. 10. The flow created by the present experimental system is shown using the square symbols.

For a given initial geometry, the fluid velocity reaches a maximum for optimum values of the thickness (Fig. 10(a)). Note that by changing the cilia thickness within the range (600, 1200) nm, the magnetic and fluid number change within the ranges $M_n = (0.63, 0.15)$ and $F_n = (4.1 \times 10^{-2}, 5.1 \times 10^{-3})$. At larger thickness the cilia are very stiff and the area swept by the cilia is smaller. This causes the flow to decrease at large thickness. As the thickness is reduced the cilia sweep a larger area and the fluid velocity increases. However, at small thickness, when the cilia are compliant (with respect to the magnetic field), they nicely follow the applied magnetic field during the effective stroke until the tip of the cilia is close to the bottom boundary. The cilia remain in this position for a fraction of the beat cycle due to the hydrodynamic interactions, while the magnet maintains to rotate. This causes the cilia to fail to catch-up with the rotating magnetic field, causing them to sweep a smaller area at lower thickness. The value of thickness at which the maximum velocity occurs decreases with increasing values of a. The increase of velocity with increase of a at lower thickness can be understood as follows. When a is increased, the cilia become more curved. The cilia no longer remain for long time near the bottom boundary between the effective and recovery strokes. This causes them to sweep a larger area as a is increased, generating a higher net flow. This mechanism is also responsible for the initial increase in the velocity with a at large thickness. In these cases, on further increase of a, the mean velocity decreases, because the cilia return to the initial position by performing the recovery stroke with higher velocity.

The dependence on the magnetization is studied by changing the magnetic number M_n (see Fig. 10(b)). For $a = 0.7$, the flow reaches a maximum value at $M_n \approx 0.6$ (corresponding to a magnetization of 2 MA m^{-1}) and a cilia thickness of 1 micron (Fig. 10(b)). It is important to note that the fluid transported is very sensitive to any changes in the magnetization at high M_n. At high values of M_n, the large magnetic field caused by the magnet causes the cilia to come very close to the substrate when it moves towards the substrate. In this situation, hydrodynamic forces prevent a quick return of the cilia. As a result, the cilia remain idle for a significant amount of time during each cycle and sweep a smaller area, leading to a decrease in the net propulsion velocity.

5 Conclusions

We have shown that fluid transport caused by the magnetically-actuated artificial cilia studied is due to a balanced combination from the shape asymmetry of the ciliary beat and fluid inertial forces. The fluid inertia increases the net fluid transport by decreasing the velocity during the recovery stroke, while increasing the velocity during the effective stroke. An intriguing feature of the system (inherently different from initial computational design studies[10,11,14]) is that the cilia tips rotate clockwise while the actuating magnet rotates counter-clockwise. This is a direct consequence of the non-uniformity of the magnetic field caused by the permanent magnet. A parametric study conducted indicates that the fluid transport is already in the optimal range with respect to the cilia

thickness, while it can be further enhanced by using a higher magnetization of the actuating permanent magnet.

Acknowledgements

This work is a part of the 6th Framework European project 'Artic', under contract STRP 033274.

References

1 M. G. H. M. Baltussen, P. D. Anderson, F. M. Bos and J. M. J. den Toonder, Inertial flow effects in a micro-mixer based on artificial cilia, *Lab Chip*, 2009, **9**(16), 2326–2331.
2 J. Belardi, N. Schorr, O. Prucker and J. Ruhe, Artificial cilia: Generation of magnetic actuators in microfluidic systems, *Adv. Funct. Mater.*, 2011, **21**(17), 3314–3320.
3 J. Den Toonder, F. Bos, D. Broer, L. Filippini, M. Gillies, J. De Goede, T. Mol, M. Reijme, W. Talen, H. Wilderbeek, V. Khatavkar and P. Anderson, Artificial cilia for active micro-fluidic mixing, *Lab Chip*, 2008, **8**(4), 533–541.
4 J. M. J. den Toonder and P. R. Onck, Microfluidic manipulation with artificial/bioinspired cilia, *Trends Biotechnol.*, 2013, **31**(2), 85–91.
5 B. A. Evans, A. R. Shields, R. Lloyd Carroll, S. Washburn, M. R. Falvo and R. Superfine, Magnetically actuated nanorod arrays as biomimetic cilia, *Nano Lett.*, 2007, **7**(5), 1428–1434.
6 F. Fahrni, M. W. J. Prins and L. J. Van IJzendoorn, Micro-fluidic actuation using magnetic artificial cilia, *Lab Chip*, 2009, **9**(23), 3413–3421.
7 E. M. Gauger, M. T. Downton and H. Stark, Fluid transport at low Reynold's number with magnetically actuated artificial cilia, *Eur. Phys. J. E*, 2009, **28**(2), 231–242.
8 J. Hussong, N. Schorr, J. Belardi, O. Prucker, J. Ruhe and J. Westerweel, Experimental investigation of the flow induced by artifiial cilia, *Lab Chip*, 2011, **11**(12), 2017–2022.
9 S. N. Khaderi, M. G. H. M. Baltussen, P. D. Anderson, J. M. J. den Toonder and P. R. Onck, The breaking of symmetry in microfluidic propulsion driven by artificial cilia, *Phys. Rev. E: Stat., Nonlinear, Soft Matter Phys.*, 2010, **82**(2), 027302.
10 S. N. Khaderi, M. G. H. M. Baltussen, P. D. Anderson, D. Ioan, J. M. J. den Toonder and P. R. Onck, Natureinspired microfluidic propulsion using magnetic actuation, *Phys. Rev. E: Stat., Nonlinear, Soft Matter Phys.*, 2009, **79**(4), 046304.
11 S. N. Khaderi, C. B. Craus, J. Hussong, N. Schorr, J. Belardi, J. Westerweel, O. Prucker, J. Ruhe, J. M. J. den Toonder and P. R. Onck, Magnetically-actuated artificial cilia for micro-fluidic propulsion, *Lab Chip*, 2011, **11**(12), 2002–2010.
12 S. N. Khaderi, J. M. J. den Toonder and P. R. Onck, Microfluidic propulsion by the metachronal beating of magnetic artificial cilia: a numerical analysis, *J. Fluid Mech.*, 2011, **688**, 44–65.
13 S. N. Khaderi, J. M. J. den Toonder and P. R. Onck, Fluid flow due to collective non-reciprocal motion of symmetrically-beating artificial cilia, *Biomicrofluidics*, 2012, **6**, 014106.
14 S. N. Khaderi, J. M. J. den Toonder and P. R. Onck, Magnetically actuated artificial cilia: The effect of fluid inertia, *Langmuir*, 2012, **28**(20), 7921–7937.
15 S. N. Khaderi and P. R. Onck, Fluid-structure interaction of three-dimensional magnetic artificial cilia, *J. Fluid Mech.*, 2012, **708**, 303–328.
16 K. Oh, J. H. Chung, S. Devasia and J. J. Riley, Bio-mimetic silicone cilia for microfluidic manipulation, *Lab Chip*, 2009, **9**(11), 1561–1566.
17 A. R. Shields, B. L. Fiser, B. A. Evans, M. R. Falvo, S. Washburn and R. Superfine, Biomimetic cilia arrays generate simultaneous pumping and mixing regimes, *Proc. Natl. Acad. Sci. U. S. A.*, 2010, **107**(36), 15670–15675.
18 J. V. I. Timonen, C. Johans, K. Kontturi, A. Walther, O. Ikkala and R. H. A. Ras, A facile template-free approach to magnetodriven, multifunctional artificial cilia, *ACS Appl. Mater. Interfaces*, 2010, **2**(8), 2226–2230.
19 R. van Loon, P. D. Anderson and F. N. van de Vosse, A fluid-structure interaction method with solid-rigid contact for heart valve dynamics, *J. Comput. Phys.*, 2006, **217**(2), 806–823.
20 C. L. van Oosten, C. W. M. Bastiaansen and D. J. Broer, Printed artificial cilia from liquid-crystal network actuators modularly driven by light, *Nat. Mater.*, 2009, **8**(8), 677–682.
21 M. Vilfan, A. Potocnik, B. Kavcic, N. Osterman, I. Poberaj, A. Vilfan and D. Babic, Self-assembled artificial cilia, *Proc. Natl. Acad. Sci. U. S. A.*, 2010, **107**(5), 1844–1847.

